



HAL
open science

Molecular dynamics simulation of cancer cell membrane perforated by shockwave induced bubble collapse

Nguyen Hoang Linh, Viet Hoang, Mai Suan Li, Junmei Wang, Philippe Derreumaux, Thi Ly Mai, Phuong H Nguyen

► To cite this version:

Nguyen Hoang Linh, Viet Hoang, Mai Suan Li, Junmei Wang, Philippe Derreumaux, et al.. Molecular dynamics simulation of cancer cell membrane perforated by shockwave induced bubble collapse. *The Journal of Chemical Physics*, 2022, 10.1063/5.0105675 . hal-03878999

HAL Id: hal-03878999

<https://hal.science/hal-03878999v1>

Submitted on 30 Nov 2022

HAL is a multi-disciplinary open access archive for the deposit and dissemination of scientific research documents, whether they are published or not. The documents may come from teaching and research institutions in France or abroad, or from public or private research centers.

L'archive ouverte pluridisciplinaire **HAL**, est destinée au dépôt et à la diffusion de documents scientifiques de niveau recherche, publiés ou non, émanant des établissements d'enseignement et de recherche français ou étrangers, des laboratoires publics ou privés.

Molecular dynamics simulation of cancer cell membrane perforated by shockwave induced bubble collapse

Nguyen Hoang Linh¹, Viet Hoang Man², Mai Suan Li^{1,3}, Junmei Wang², Philippe Derreumaux^{4,5}, Thi Ly Mai⁵, Phuong H. Nguyen^{5*}

¹*Institute for Computational Science and Technology,
SBI Building, Quang Trung Software City,
Tan Chanh Hiep Ward, District 12 ,
Ho Chi Minh City, Vietnam*

²*Department of Pharmaceutical Sciences,
School of Pharmacy, University of Pittsburgh,
Pittsburgh, PA 15213, USA*

³*Institute of Physics, Polish Academy of Sciences,
Al. Lotnikow 32/46, 02-668 Warsaw, Poland*

⁴*Institut Universitaire de France (IUF)*

⁵*CNRS, Université de Paris, UPR9080,
Laboratoire de Biochimie Théorique,
Institut de Biologie Physico-Chimique,
Fondation Edmond de Rothschild,*

13 rue Pierre et Marie Curie, 75005 Paris, France

(Dated: November 21, 2022)

It has been widely accepted that cancer cells are softer than their normal counterparts. This motivates us to propose, as a proof-of-concept, a method for the efficient delivery of therapeutic agents into cancer cells while normal cells are less affected. The basic idea of this method is to use a water jet generated by collapse of the bubble under shockwave to perforate pores in the cell membrane. Given a combination of shockwave and bubble parameters, the cancer membrane is more susceptible to bending, stretching and perforating than the normal membrane because bending modulus of the cancer cell membrane is smaller than that of the normal cell membrane. Therefore, therapeutic agent delivery into cancer cells is easier than in normal cells. Adopting two well-studied models of the normal and cancer membranes, we perform shockwave induced bubble collapse molecular dynamics simulations to investigate the difference in response of two membranes over a range of shockwave impulse 15-30 mPa.s and bubble diameter 4-10 nm. The simulation shows that the presence of bubble is essential for generating water jet which is required for perforation, otherwise pores are not formed. Given a set of shockwave impulse and bubble parameters, the pore area in the cancer membrane is always larger than that in the normal membrane. But too strong shockwave and/or too large bubble results in too fast disruption of membranes, and pore areas are similar between two membrane types. The pore closure time in the cancer membrane is slower than that in the normal membrane. The implications of our results for applications in real cells are discussed in some details. Our simulation may be useful for encouraging future experimental work on novel approaches for cancer treatment.

I. INTRODUCTION

The plasma cell membrane regulates the entry and exit of substances via specific mechanisms. Small substances, such as ions, sugars and amino acids can cross the membrane via ion channels or protein pumps. Macromolecules must be carried into cells by membrane bound vesicles through the endocytosis mechanism[1]. These two mechanisms limit the entry of molecules which are not naturally needed by cells. As a consequence, although a large number of drugs is available for treating cell diseases, only a few drugs are used if they can cross the cell membrane. Therefore, a number of approaches has been proposed aimed at enhancing the transport of drugs through the cell membrane. Two well-known, vi-

ral and chemical methods, have been developed but they are still limited by the low efficiency and toxicity. As a remedy, the physical approach has been recently proposed for highly efficient drug delivery with low toxicity. The basic idea of the physical approach is to create transient pores in the cell membrane, called poration, where drugs can penetrate into cell easier. Physical methods include photoporation, electroporation, magnetoporation and mechanoporation which use different kind of physical forces such as magnetic, thermal, mechanical and electrical forces to open the pore. For an excellent review of the drug delivery methods, readers are referred to recent publication[2]. Among these methods, the mechanoporation using the shockwave force is promising because it can rapidly deliver large macromolecules into cells in a local, noninvasive and cost effective manner[3]. For examples, Kodama et al. used shockwave to deliver large cytoplasmic molecules into cells. The authors suggested that the shear force generated by the shockwave temporarily af-

* Corresponding author: nguyen@ibpc.fr

fects the permeability of the membrane, and the impulse of the shockwave plays an important role in governing the permeability. This method can deliver large macromolecules of up to 2×10^6 molecular weight into cells[4]. Recently, Lopez-Marin et al. have studied the shockwave induced damage and poration in cell line HEK293 and tumor-derived cell line MCF-7, and results from scanning electron microscopy revealed transient hole-like structures after shockwave exposure. The authors also showed differences in membrane permeability of two cell lines[5]. Qi et al. showed that shockwave can trigger the release of ATP from osteosarcoma U2OS cells by increasing the membrane permeability[6]. The ability of shockwave to enhance the delivery of very large molecules suggests that shockwave should also be a promising method in gene therapy and protein delivery[7, 8]. We should mention that the shockwave has been used in other medical applications. For example, high energy shockwaves have been used for more than 30 years to disintegrate urolithiasis. Extracorporeal shockwave therapy has been clinically used for many musculoskeletal conditions. It has been suggested that shockwave accelerates tissues regeneration, reduces calcification and inhibits pain receptors [9].

To further develop this sensitive method aimed at enhancing drug delivery into cancer cells, one needs a better understanding of the mechanism of shockwave interacting with the cell membrane, especially at the molecular level. Unfortunately, it is very difficult to observe experimentally the direct interaction between shockwave and membranes due to the short time scale on the order of picoseconds, and small length scale of several nanometers. Therefore, several studies have employed molecular dynamics (MD) simulations to investigate the molecular mechanism of the shockwave induced membrane damages, with and without bubbles[10–23]. Koshiyama et al. performed for the first time an all-atom nonequilibrium MD simulation under a shockwave but without bubbles and observed the penetration of waters into the hydrophobic region of the membrane, which was caused by a decrease in membrane thickness[10]. Choubey et al. performed large-scale all-atom MD simulations of lipid membranes with shockwave and nanobubbles and showed that the bubble collapse generates shear flow of water on membrane leaflets and pressure gradients across them, creating transient nanochannels through which water molecules translocate across the membrane[11]. Steinhäuser and colleagues developed an advanced large and multi-scales coarse-grained simulation method using dissipative particle dynamics, and applied it to study effects of shockwave on DPPC membranes. The authors obtained a threshold shock front velocity, below which the membrane recovers from shockwave induced damage, and above that the membrane could not be recovered[12–15]. Santo et al. employed coarse-grained MD simulation to study the impact of shockwave and bubbles on the damage and recovery of lipid membranes. Interestingly, they showed that not every lipid molecule remained in the bi-

layer after recovery, some lipids moved out into water and created micelles[16, 17]. Adhikari et al. showed that in the absence of bubbles, high intensity shockwaves do not induce pores on membranes, but weaker impulses can lead to membrane poration in the presence of bubbles[18]. Similarly, Lu et al. performed MD simulation of the shockwave induced delivery of paclitaxel drug through a lipid membrane and showed that the paclitaxel molecule can penetrate the membrane only under the joint effect of the shockwave and nanobubble[20]. Sun et al. simulated the shockwave induced collapse of lipid-shelled nanobubbles and interestingly, they showed that compared with the cases of vacuum nanobubbles, the lipid nanobubbles could weaken the effects of shock waves[19]. Nan et al. performed coarse-grained MD simulation of the shockwave induced bubble collapse and observed not only membrane perforation but also the occurrence of nanoscale cavitation during the perforation process[21]. Hu et al. analyzed effects produced by the collapse of multiple nanobubbles in the vicinity of biomembranes in the presence of an electric field by MD simulation[22], and showed that multiple nanobubbles make it possible to create larger pores on the membrane[22]. Very recently, Wei et al. studied the impact of shockwave induced bubble collapse on the damage of cell membranes with different lipid peroxidation levels, and showed that the pore sizes increase with the peroxidation level[23]. One of important findings obtained from all these simulation studies is that the shockwave alone does not have much impact on membranes, but the presence of gas bubbles, which pre-exist or are nucleated during the shockwave propagation, plays an essential role in the membrane poration.

Our main interest is the application of the shockwave in combination with bubble in the drug delivery for cancer treatment. To date cancer treatments, including surgery, radiotherapy and chemotherapy are widely used. Extensive resection followed by adjuvant chemoradiotherapy seems to be the only treatment that modifies the survival of cancer patients. However, with the chemotherapy, the therapeutic agent affects not only cancer cells but also normal cells, causing severe side effects. Therefore, novel therapeutic methods are needed to minimize side effects on the normal cells. Our core aim is to develop such a method, based on the difference in the mechanical properties of normal and cancer membranes. Recently, a number of studies has shown that cancer cells from a large number of different organs are softer than their normal counterparts[24]. Therefore, in recent years, mechanical properties of cancer cells have been suggested as biomarkers for early cancer diagnosis, targeted for the prediction, treatment and even prevention of cancer[25]. Our research hypothesis is that if cancer cells are softer than normal cells, then we can choose shockwaves with appropriate impulses and bubbles with suitable sizes so that under the shockwave induced bubble collapse, the cancer cell membrane is maximally perforated while the normal cell membrane is minimally affected. Therefore,

therapeutic agents are maximally delivered into cancer cells but minimally into normal cells.

In a previous work, we performed equilibrium MD simulations to study the elastic properties of normal cell membranes and cancer cell membranes[26]. In our simulations models, normal cell membranes have a highly asymmetric lipid composition[27], where the extracellular leaflet is mainly composed of phosphatidylcholine (PC) and sphingolipids and the intracellular leaflet is mostly composed of phosphatidylethanolamine (PE) and phosphatidylserine (PS) lipids. When normal membranes are transformed to cancer membranes the concentration of the negatively charged PS lipids is increased in the extracellular leaflet[28, 29], and the cholesterol (CHL) concentration is reduced[30]. We calculated the elastic moduli including bending, tilt and twist constants of the normal and cancer membranes. The results showed that at low cholesterol concentrations, all elastic moduli become smaller, implying that the cancer membrane is indeed softer than the normal counterpart.

In this work, we carry out nonequilibrium MD simulations of shockwave induced bubble collapse of a normal membrane and a cancer membrane whose structures are known from our previous work[26]. We vary the shockwave impulses and bubble diameters over a wide range of values to observe the difference in response of the normal and cancer membranes. The main finding is that given a combination of a shockwave and a bubble, the cancer membrane is more bent, stretched and perforated than the normal counterpart.

II. METHODOLOGY

A. The membrane models

Lipid	Normal membrane		Cancer membrane	
	outer	inner	outer	inner
SM	336	96	216	216
DOPC	368	112	240	240
DOPE	112	368	240	240
DOPS	0	240	120	120
CHL	408	408	204	204

Table I. The total number of each lipid component in the outer and inner leaflets of the normal and cancer membrane models. The cancer membrane model is obtained by symmetrising the number of lipids between the outer and inner leaflets of the normal membrane model.

In a previous work[26], we carried out all-atom MD simulations of five normal membrane models and five cancer membrane models. The cancer membranes were taken into account the overexpression of PS lipids in the outer leaflet and the reduction of cholesterol concentration. Results showed that at the same cholesterol concentration the bending moduli of the normal

and cancer membranes are very similar. This indicates that the overexpression of the PS lipids does not affect significantly the elasticity of the normal or cancer membranes. At low cholesterol concentrations, all elastic moduli become smaller, implying that the reduction in cholesterol in cancer membranes could contribute, at least partly to the softening of cancer cells. Therefore, in this work, we consider only two membrane models among the ten membrane models used in previous work[26]: a normal membrane model and a cancer membrane model which differ in the PS lipids concentration in the outer leaflets, and in the cholesterol concentration. Each model contains four lipid types: 1,2-dioleoyl-sn-glycero-3-phosphocholine (DOPC), sphingomyelin lipids (SM), 1,2-dioleoyl-sn-glycero-3-phosphoethanolamine (DOPE) and 1,2-dioleoyl-sn-glycero-3-phospho-L-serine (DOPS) lipids. For each model, we take the last equilibrium membrane structure at 2 μ s obtained from previous simulations[26], and translate it along the x and y -axis to obtain a doubled size membrane with lengths $(x, y) = (24, 24)$ nm. This guarantees that the new membrane structure is in the equilibrium state, and large enough to accommodate large bubbles having diameters of ~ 10 nm. The numbers of lipids and cholesterol of two membrane models are listed in Tab.I.

B. Shockwave induced bubble collapse simulation method

In this work, we employ the shockwave method originally developed by Koshiyama et al.[10]. The sketch of the simulation setup is shown in Fig.1. The system is a rectangular prism box composed of two lipid membranes described above, a bubble and the whole system is solvated in water. We are interested in the lower membrane, while the upper membrane is only technically used to prevent the shockwave coming back to another side of the lower membrane due to the periodic boundary condition used in the simulation[31, 32]. The distance between the membrane and the bubble is d_{mb} , and the diameter of the bubble is d_b . To generate a shockwave with an impulse I , an excess momentum $M = I \times A$ is applied to a slab of waters with a volume of $A \times d_s$. Here, A and d_s are the area in the (x, y) plane and the thickness of the water slab, respectively. Initially, the distance between the slab of water and the bubble is d_{bs} .

The all-atom CHARMM36 force field[33] and the TIP3P water model are used to model the lipids and solvent, respectively. The initial dimensions of the primary unit cell are $(x, y, z) = (24, 24, 54)$ nm, consisting of 3.112.724 atoms in total. Starting from the initial structure of the normal membrane or cancer membrane, an equilibrium MD simulation is carried out for 100 ns in the NPT ensemble at the pressure $P_0 = 1$ bar and temperature $T = 300$ K. Then, we take the last ten equilibrium structures separated by 100 ps, and for each structure we remove water molecules in the spherical region hav-

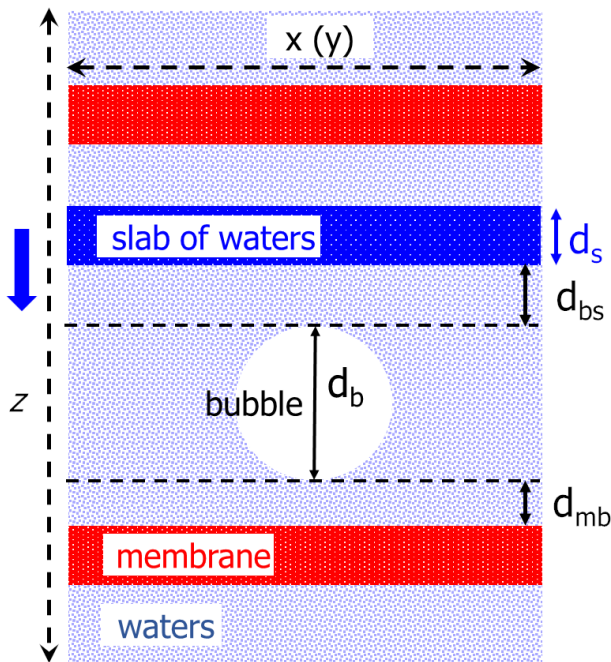


Figure 1. Sketches of the shockwave induced bubble collapse simulation method. The rectangular prism box with lengths (x, y, z) contains two membranes and a bubble solvated in water. A slab of waters with a volume of $x \times y \times d_s$ is selected for the shockwave generation. A bubble with a diameter d_b is placed at a distance of d_{mb} above the membrane. The distance between the water slab and the bubble is d_{bs} .

ing diameter d_b near the lower membrane. This empty water space mimics a bubble. In this work, we consider four bubble sizes with $d_b = 4, 6, 8, 10$ nm. These membrane/bubble systems are used as initial structures for the shockwave simulations. The shockwave I defined as the time integral of pressure over the shock pulse duration is varied from $I = 15$ mPa.s to $I = 25$ mPa.s. The shockwave induced bubble collapse MD simulation is performed by using the GROMACS simulation package[34] in the NVE ensemble. The equations of motion are integrated using the leapfrog algorithm with a small time step of 0.5 fs. The small time step is used to ensure the stability of the simulations. The electrostatic interactions are calculated using the particle mesh Ewald method and a cutoff of 1.2 nm [35], and the forces switched to zero from 1.0 to 1.2 nm are used for the van der Waals interactions. The nonbonded pair lists are updated every 5 fs. Each simulation is run for 50 ps and the data is saved for every 500 MD steps (every 0.25 ps) for subsequent analyses.

C. Data analysis

In our simulations the shockwave moves in the z -direction, thus to monitor the propagation, we calculate profiles of the normal pressure component, $P_{zz}(z)$, and

temperature, $T(z)$. To this end, we discretise the simulation box in thin slabs of width 0.5 nm which are oriented parallel to the xy -plane. By computing the average pressure and temperature in each slab, the propagation can be monitored in details. Here, pressure is calculated by using the method developed by Ollila et al.[36], and temperature is directly calculated from velocity of atoms.

To measure the membrane pore area ΔS , we place a 2D grid with the size of each grid square of (0.1×0.1) nm on the (x, y) membrane surface, and count the squares on the grid having zero lipid atoms[18, 23].

The order parameters of the lipid acyl chain tails are calculated as $S_i = \langle 3 \cos^2 \theta_i - 1 \rangle / 2$, where θ_i is the angle between the i -th C-H bond vector and the bilayer normal[37], and the angular brackets represent ensemble average over all lipids.

III. RESULTS

We have performed MD simulations to investigate the difference in response of the normal and cancer cell membranes to the shockwave induced bubble collapse. There are five parameters in the simulation setup including the shockwave impulse I , diameter of bubble d_b , distance from bubble to membrane d_{mb} , distance from water slab to bubble d_{bs} , and thickness of water slab d_s [Fig.1]. Among these, two physical parameters that can be controlled experimentally are the shockwave impulse I and bubble size d_b . The other parameters d_{mb}, d_{bs}, d_s are merely parameters defined only in the simulation. Thus, in this study, we only choose appropriate values, $d_{mb} = 1$ nm, $d_{bs} = 2$ nm and $d_s = 3$ nm for all simulations and values of I and d_b are varied to obtain different responses in the membranes. We note that two membranes are used in simulations but as explained above we are only interested in the lower membrane [Fig.1] whose results are presented below. For each simulation, ten trajectories are carried out starting from different initial structures and results are presented as an ensemble average over all trajectories.

A. Shockwave induced bubble collapse and membrane response

To describe the shockwave propagation, the collapse of the bubble and the response of the membrane in details, let us consider a representative simulation of the normal membrane using a shockwave impulse $I = 21$ mPa.s and a bubble with diameter $d_b = 10$ nm. We calculate various quantities including the vector field of velocity of atoms, the profiles of the pressure, kinetic energy, temperature and mass density. To provide an intuitive picture, snapshots are also visualised. These results are shown in Fig.2 and Fig.3.

By construction, all atoms within the water slab above the bubble [Fig.1] are initially assigned to the same high

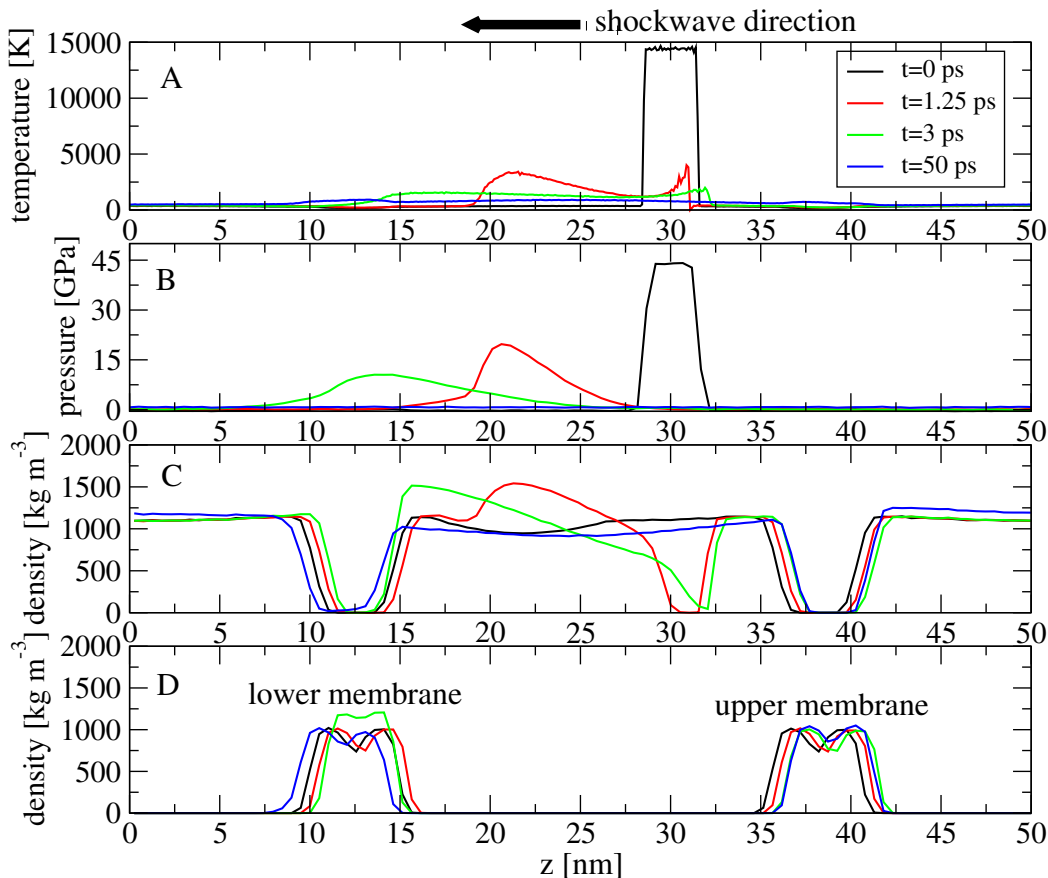


Figure 2. The profiles along the z -axis of the temperature (A), normal pressure component (B), mass density of water (C) and mass density of membrane (D) obtained at 0 ps (black), 1.25 ps (red), 3 ps (green) and 50 ps (blue). Shown are results obtained from the simulation of the normal membrane using a shockwave impulse $I = 21$ mPa.s and a 10 nm bubble.

velocity V , which is calculated as $V = (I \times A)/(m \times N)$ [10]. With the impulse $I = 21$ mPa.s, the area of the water slab $A = 576$ nm², the weight of a water molecule $m = 18$ g/mol and the number of water molecules in that slab $N = 58044$ we obtain $V \sim 9$ km/s with direction parallel to the z -axis and towards to the membrane. This results in an excess high temperature of ~ 15000 K and a pressure of ~ 44 GPa in the water slab at $t = 0$ ps [Figs.2A,B]. These water atoms then move extremely fast toward the membrane as seen from the velocity vector field in Fig.3A. This causes an increase in water density profile in the direction of the membrane with the maximum values of 1532 kg/m³ at $t \sim 1.25$ ps, $z \sim 21$ nm and 1519 kg/m³ at $t \sim 3$ ps, $z \sim 15$ nm, thus leaving an empty space behind them at the initial position of water slab ($z \sim 30$ nm) [Fig.2C and Fig.3B]. This is because the initial equilibrated water molecules at 300 K above the water slab are not quick enough to occupy the space left by the water in the slab. As a consequence, the temperature and pressure in the water slab are reduced significantly from the initial values, and increased quickly in the direction of the membrane, reaching the maximum values of ~ 3400 K and 20 GPa, respectively at $t \sim 1.25$

ps and $z \sim 21$ nm [Fig.2A,B]. Along the way, a part of water in the slab enters the empty space of the bubble without any obstacle, mimicking the bubble collapse. At $t = 1.25$ ps, the bubble is partially collapsed [Fig.3B] but the membrane has not been affected yet, thus the average kinetic energy of the membrane is still maintained at an equilibrium value of ~ 4 -5 kJ/mol, uniformly distributed over all lipids [Fig.3C], and the temperature is still around the initial value of ~ 300 K [Fig.2A]. In contrast, the propagation of the part of waters in the slab, which do not enter the bubble, is slower due to the resistance of the water below the slab. The difference in velocity between these two parts of water, i.e. one enters the bubble and one outside the bubble, produces high-speed water jet directed towards the membrane as shown by the velocity vector field in Fig.3A. After entering the bubble, the water jet continues to propagate, and occupies completely the bubble space at $t \sim 3$ ps, mimicking the full collapse of the bubble [Fig.3E]. Then, it hits the lipid membrane and velocity drops down to ~ 6 km/s with the velocity vector field shown in Fig.3D. The membrane area located just below the bubble receives directly the kinetic energy from the water jet, thus its tempera-

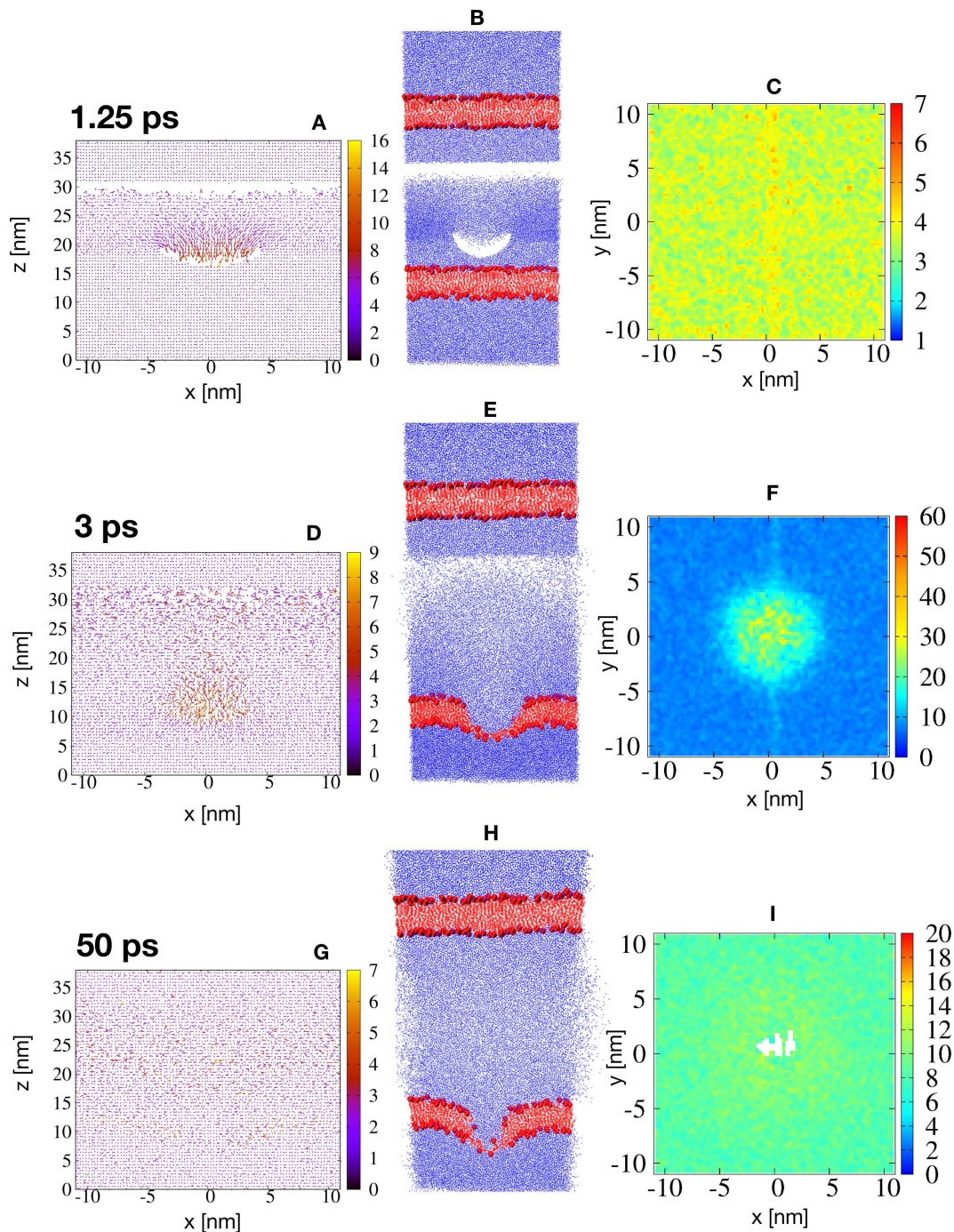


Figure 3. The velocity field (in km/s) of atoms projected on the (x,z) plan (left panels), the snapshot of the system (middle panels) and the kinetic energy (in kJ/mol) map of atoms projected on the (x,y) plan (right panels). Shown are results at 1.25, 3 and 50 ps for the normal membrane simulated with a shockwave impulse of 21 mPa and a 10 nm in diameter bubble. In the snapshots, the water and membrane are shown in blue and red colours, respectively. The white area in the panel I indicates the pore.

ture and pressure at the membrane surface ($z \sim 15$ nm, Fig.2D) increase to ~ 1600 K and ~ 10 GPa, respectively [Fig.2A,B], and the kinetic energy at the focal point of the membrane increases to ~ 40 kJ/mol [Fig.3F]. The kinetic energy of the remaining part of the membrane is slightly increased to ~ 10 kJ/mol. This causes the

deformation of the membrane area just below the bubble [Fig.3E]. After that, the water jet is thermalised and its kinetic energy is redistributed, leading to increase in kinetic energy of ~ 14 kJ/mol of surrounding water and lipid molecules. Their velocities are randomly distributed as shown by the velocity vector field and kinetic energy

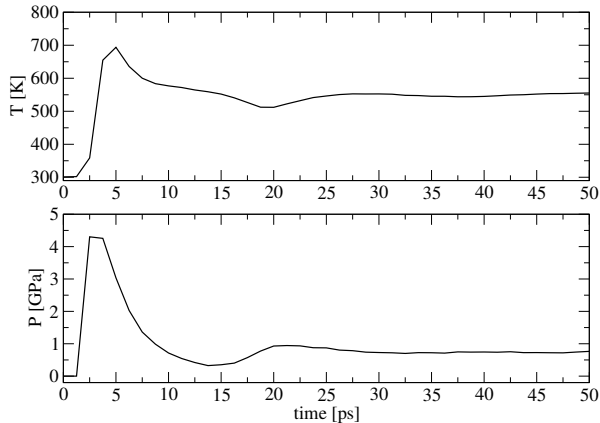


Figure 4. Time dependence of the average temperature (upper panel) and normal pressure (lower panel) across membrane surface along the z direction. Shown are results obtained from the simulation of the normal membrane using a shockwave impulse $I = 21$ mPa.s and a 10 nm bubble.

map in Figs.3G, I, respectively at 50 ps. The membrane is now highly stretched and pores are formed [Figs.3H, I]. We note that the membrane is basically not translated under shockwave as seen from the position z of the membrane density profile shown in Fig.2D. This is due to the use of two membranes technique in our simulation as described above.

Next, we calculate the average temperature and normal pressure across membrane surface as a function of time and results are shown in Fig.4. The temperature remains at the initial value of ~ 300 K until the arrives. Upon the arrival, the temperature increases sharply to a maximum values of ~ 700 K at ~ 5 ps, then it slowly decreases and reaches ~ 560 K at 50 ps. Similarly, there is a sharp increase in pressure from the initial value $\sim 10^{-4}$ GPa (1 bar) to the maximum value of 4.2 GPa at ~ 5 ps, followed by a rapid decrease of pressure which reaches a minimum value of ~ 0.35 GPa at 13 ps and then the pressure rises again toward the final value of ~ 0.73 GPa at 50 ps. We should mention that the shockwave induced bubble collapse simulation is carried out in the NVE ensemble, and the very high initial kinetic energy of the shockwave is redistributed over all atoms, thus the temperature and pressure of the membrane do not relax to the initial values of 300 K and 1 bar, respectively. Of note, we analysed trajectories simulated with different shockwave impulses and bubble sizes, and found that the mechanism of bubble collapse and membrane response is similar for all simulations.

It is of interest to compare the targeted impulse I , which is used to generate the initial shockwave, with actual pressure impulse exerted by the shockwave on the membrane. From the pressure profile $P(t)$ shown in

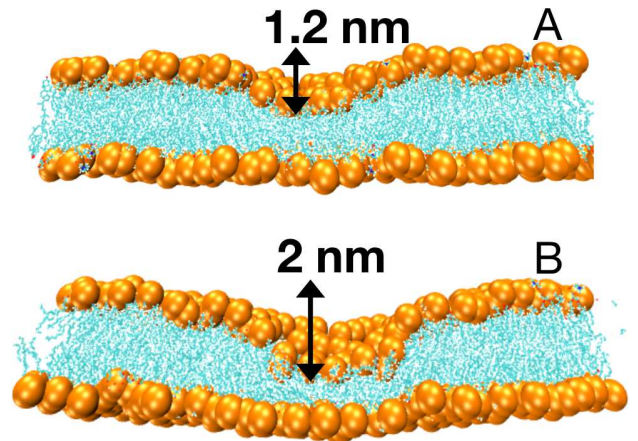


Figure 5. Snapshots taken at $t = 3$ ps from the simulation of the normal (A) and cancer (B) membranes with a bubble having a diameter of 10 nm and a shockwave impulse of 15 mPa.s. The phosphate atoms of lipids are shown in orange and other atoms are in cyan. The bending values of the membranes are indicated.

Fig.4, the pressure impulse on the membrane is calculated as $I_{\text{mem}} = \int_0^t P(\tau) d\tau$, where t is the time duration of the positive phase of the shockwave[10]. The results are shown in Tab.II for the simulations using with a 10 nm bubble and different targeted impulses I . As seen,

I [mPa.s]	v_{slab} [km/s]	I_{mem} [mPa.s]
15	6.43	13.18 ± 0.15
17	7.28	16.01 ± 0.21
19	8.14	17.90 ± 0.18
21	9.00	19.71 ± 0.23
23	9.85	22.05 ± 0.12
25	10.71	24.56 ± 0.26

Table II. A comparison between the targeted impulse I and the actual pressure impulse I_{mem} exerted on the membrane by the shockwave induced bubble collapse. v_{slab} is the initial velocity assigned to water atoms in the water slab for a given targeted impulse. In all cases, the time duration of the positive phase of the shockwave $t = 10$ ps is used in the calculation. Shown are results obtained from the simulations of the normal membrane using a 10 nm bubble.

the actual pressure impulses are very close to the targeted counterparts, indicating that the initial impulses are not dissipated much before hitting the membrane. Therefore, the membrane is indeed impacted by the targeted impulses.

B. Response of normal and cancer membranes upon bubble collapse

Having understood the mechanism of shockwave induced bubble collapse, we now wish to investigate the

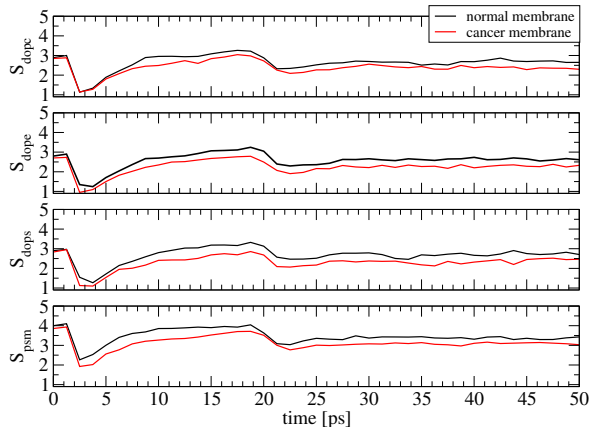


Figure 6. Time-evolution of the sum lipid order parameter S_{lipid} of the normal (black) and cancer (red) membranes obtained from a simulation using a shockwave impulse of 21 mPa.s and a bubble with a diameter of 10 nm.

response of the normal and cancer membranes in details, focusing on the membrane bending, lipid ordering and membrane pore formation. In the previous simulation we calculated the elastic moduli of the normal and cancer membranes in equilibrium state and obtained the bending modulus $K_c = 10.5 \times 10^{-20}$ J for the normal membrane and $K_c = 8.1 \times 10^{-20}$ J for the cancer membrane[26]. This means that the cancer membrane is softer than the normal membrane. This implies that under the same water jet, the cancer membrane should be deformed more than the normal membrane. To confirm this, we carry out simulations using a 10 nm diameter bubble and a relatively weak shockwave of 15 mPa.s, such that only the membrane bending, but not pore formation, is observed. To obtain a qualitatively impression, Fig.5 shows snapshots of the two membranes at $t = 3$ ps, and indeed, the cancer membrane is bent more than the normal membrane, with a bending of 2.0 nm and 1.2 nm, respectively.

To exam the response of membranes in more detail, we follow the time-evolution of the order parameters of the lipid acyl chain tails during the simulation of the normal and cancer membranes. For the DOPC, DOPE and DOPS lipids, each tail consists of 17 order parameters ($i = 1 \cdots 17$), and for PSM lipids, each tail consists of 15 order parameters ($i = 1 \cdots 15$). For simplicity, we sum all order parameters of each lipid type: $S_{\text{lipid}} = \sum_i S_i$. As an example, the time-evolution of the four S_{lipid} in the normal and cancer membranes is shown in Fig.6 for the simulations using a 10 nm diameter bubble and a shockwave of 21 mPa.s. As seen, both normal and cancer membranes are initially at equilibrium, and their order parameters are very similar. At $t \sim 3$ ps, the bubble is completely collapsed and the water jet hits the membrane. Thus the membrane is highly disturbed and lipids

become disordered. This is indicated by a largest reduction of $\sim 60\%$ in the order parameters of all lipid types at 3 - 4 ps for both membranes. Then, the intensity of the water jet is reduced because its kinetic energy is transferred to other degrees of freedom of the membrane and water. After hitting the lower membrane, the water molecules bounce back, and the membrane also tends to be pulled back to its original state as indicated by the increase in all order parameters of all lipid types from 3 ps to 18 ps. However, due to the presence of the upper membrane, the water molecules bounce back towards the lower membrane again causing the lipids to become disordered as indicated by the decrease in order parameters at $t \sim 18 - 20$ ps. Then, the kinetic energy of the water molecules is redistributed, and the oscillation of the water flow between the upper and lower membranes disappears, the membrane is stabilised, and the order parameters approach to horizontal values (see at 50 ps). Importantly, we observe that the cancer membrane is more disordered than the normal membrane. The order parameters of the cancer membrane are $\sim 14\%$ lower than that of the normal membrane [Fig.6].

To see what changes in the structure of the membrane lead to a decrease in the order parameters S_i at ~ 3 ps seen in Fig.6, we calculate the distribution of the θ_i angle between the i -th C-H bond vector and the bilayer normal for different lipid types. We found that at equilibrium these angles are mainly distributed around 0 degree, thus S_i are large. Upon hit by the water jet around 3-4 ps, the distributions of θ_i are broader due to the compressed lipids, leading to smaller order parameters. Therefore, the reduction in the order parameters is associated with the reduction in the membrane thickness.

The main aim of the shockwave induced bubble collapse method is to create pores on the cell membrane where drugs can be efficiently delivered into the cell. Therefore, the pore area is an important quantity to validate the efficiency of the method. We calculate the pore area ΔS (see Section II.C) in the normal or cancer membrane at equilibrium and obtain an area of $\Delta S \sim 3$ nm². Of course, there is no well-defined pore in an equilibrium membrane, and this value is simply the sum of all small empty spaces in the (x, y) plane of a membrane at equilibrium.

First, we investigate the dependence of the pore area on the shockwave impulse, given a bubble size. Fig.7 shows, as an example, the time evolution of the pore area induced by the collapse of a 10 nm bubble under different shockwave impulses $I = 15 - 25$ mPa.s for the normal and cancer membranes. Overall, the same feature of the time evolution of the pore area is observed for all impulses and for two membranes. At $t = 0$ ps when the water jet has not hit the membrane yet, both membranes are at equilibrium and $\Delta S \sim 3$ nm². Then, the shockwave induces the collapse of the bubble and the generated water jet hits the membranes. With $I = 15$ mPa.s, the water jet is not strong enough to perforate pores in the membrane. The membranes are slightly bent as seen from Fig.5, and

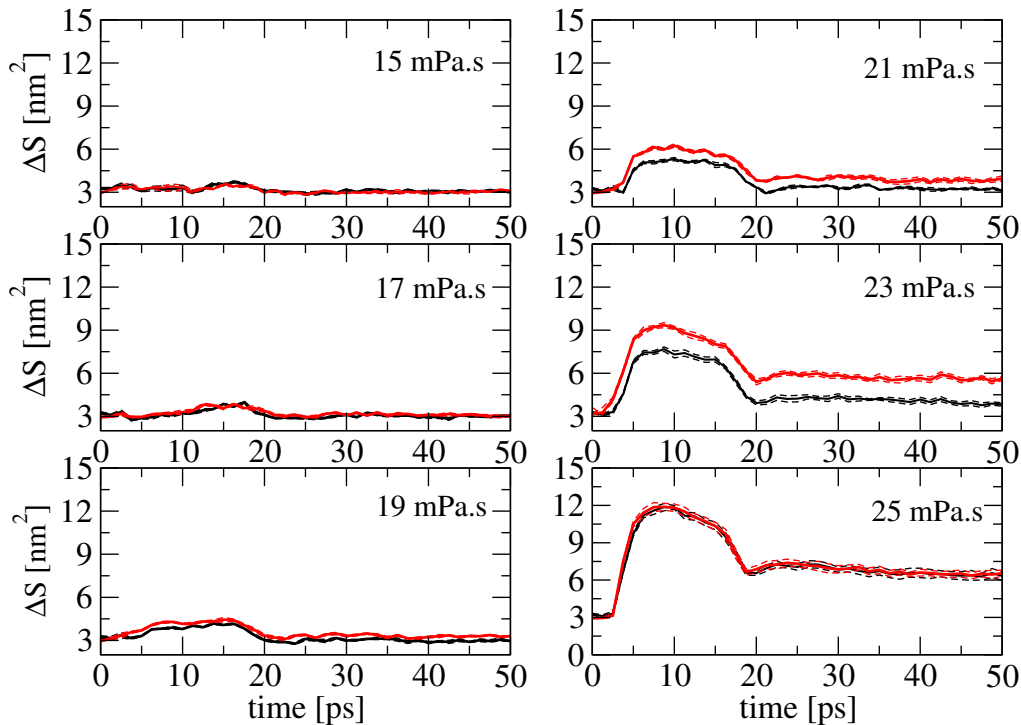


Figure 7. Time evolution of the pore area ΔS induced by the collapse of a 10 nm bubble under different shockwave impulses $I = 15 \dots 25$ mPa.s. Show are results of the normal (black lines) and cancer (red lines) membranes. The average data (over 10 trajectories) are shown by the solid thick lines and the error bars are shown by the dashed lines.

ΔS is slightly above the equilibrium value. With $I = 17$ and 19 mPa.s, the pore areas slowly increase and reach the largest values of 4-4.5 nm² around $t = 15$ ps. With stronger impulses of $I = 21, 23$ and 25 mPa.s the membranes are quickly perforated, and largest pore areas are formed around $t = 7 - 10$ ps. After that the intensity of the water jet decreases and the pores tend to close, reflected by the decrease in pore areas. After 20 ps the water jet is vanished, and the pores are fully closed as in the weak shockwave cases $I = 15 - 19$ mPa.s. However, larger pores perforated by stronger shockwave impulses $I = 21 - 25$ mPa.s are not closed after 50 ps. Clearly, for both membranes the pore area increases with the increase of the shockwave impulse. For instant, at a low impulse intensity of 19 mPa.s the maximum pore area is around 4.5 nm² but with an intensity $I = 25$ mPa.s the pore area is three times larger, around 13 nm². We note that in all cases, largest pores are formed at $t \sim 10 - 15$ ps, while the maximum reduction in the lipid order parameter occurs much faster, around 3-4 ps [Fig.6]. To explain this, we note that the membrane outer leaflet (facing the water jet) is affected immediately upon hit by the water jet, while the inner leaflet has not been affected yet [Fig.5].

Thus, at this moment the lipid order parameters, which are calculated for lipids pertaining in both leaflets, are affected. In contrast, a pore in a bilayer are fully formed only if pores are formed in both leaflets, and this process is slow.

At weak shockwave impulses $I = 15 - 17$ mPa.s, there is no difference in ΔS between the normal and cancer membranes because in these cases, pores are not really formed. At $I = 19$ mPa.s, the pore area in the cancer membrane is slightly larger than that in the normal membrane. The difference becomes more obvious with $I = 21 - 23$ mPa.s, with the maximum pore areas in the cancer membrane are 19-23% larger than that in the normal membrane. Interestingly, with $I = 25$ mPa.s, the pore areas in both membranes become very similar. This is because if the shockwave is too strong then the speed of the water jet is very high, it hits and ruptures the membrane instantaneously without membrane bending and stretching, thus the results do not depend much on the membrane elasticity. Finally, we note that the difference in the average value of ΔS between the two membranes is larger than the standard deviation values, indicating that the cancer membrane is indeed more prone to perforation

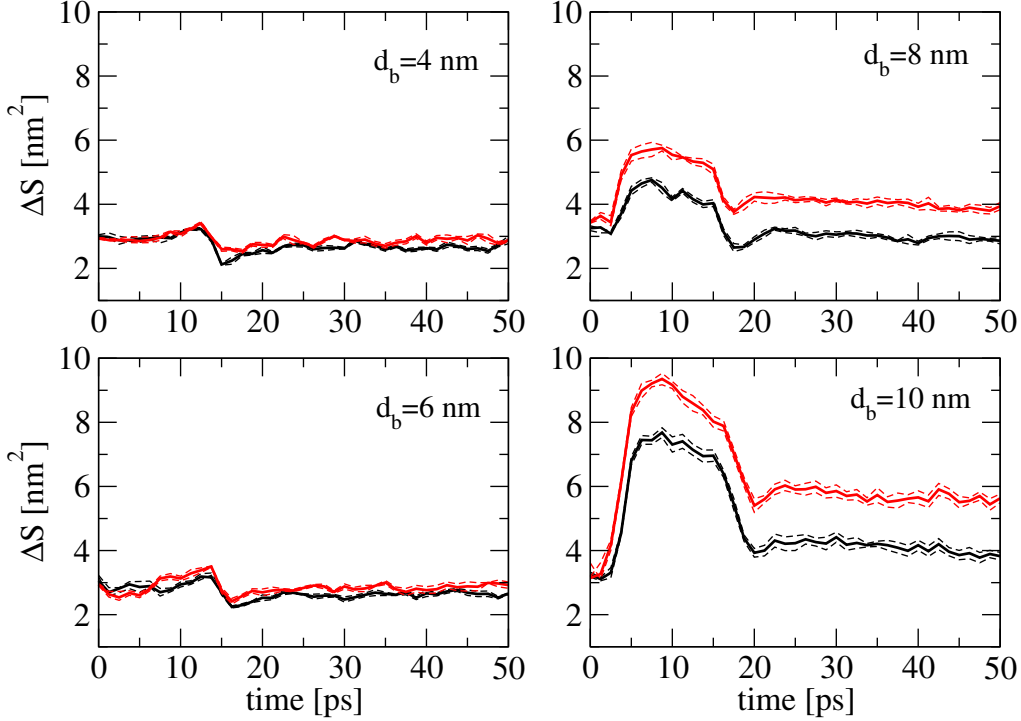


Figure 8. Time evolution of the pore area induced by the collapse of bubbles with different radius d_b under a shockwave impulse $I = 23$ mPa.s. Show are results of the normal (black lines) and cancer (red lines) membranes. The average data (over 10 trajectories) are shown by the solid thick lines and the error bars are shown by the dashed lines.

than normal membrane.

Next, we wish to investigate the dependence of the pore area on the bubble size given a shockwave impulse. Fig.8 shows the time evolution of the pore area induced by the collapse of bubbles having diameters $d_b = 4 - 10$ nm under a shockwave impulse $I = 23$ mPa.s. This impulse is chosen because the difference in the pore area between the two membranes is most obvious [Fig.7]. We note that in all cases, the shockwave impulse is the same thus the pressure exerted by the water jet on the membranes should be the same. However, it is clear that the larger the diameter of the bubble, the larger the diameter of the water jet and therefore the larger the area of the membrane impacted by the water jet. As a consequence, small bubbles with $d_b = 4$ and 6 nm induce small pores with $\Delta S \sim 3.5$ nm², while larger bubbles, $d_b = 8$ and 10 nm, create larger pore areas. Importantly, given a bubble size the pore area in the cancer membrane is always larger than that in the normal counterpart. For example, with an 8 nm bubble, the largest pore areas are 4.5 and 6 nm² for the normal and cancer membranes, respectively. After 50 ps, these areas decrease to ~ 3 and 4 nm², indicating that the pore in the normal membrane is closed but that

is still opened in the cancer membrane. Similar results are observed for the 10 nm bubble case [Fig.8].

In summary, the above results show that (i) given the same bubble, a stronger shockwave impulse induces a larger pore area in the membrane, (ii) for a given shockwave impulse, a larger bubble induces a larger pore in the membrane, (iii) for a given set of the bubble and the shockwave parameters, the pore area in the cancer membrane is always larger than the pore area in the normal membrane, and (iv) if the shockwave impulse is too strong then the pore areas in the normal and cancer membranes become similar.

C. Pore closure

As shown above, the pore in a membrane induced by weak shockwave impulse or by collapse of a small bubble is quickly closed. For example, with a weak impulse of 15 mPa.s or a small 4 nm bubble, the pore area reaches the maximum value ~ 3.5 nm² then quickly decreases to the initial equilibrium value of ~ 3 nm² [Figs.5,8]. However, with stronger impulses and/or bigger bubbles

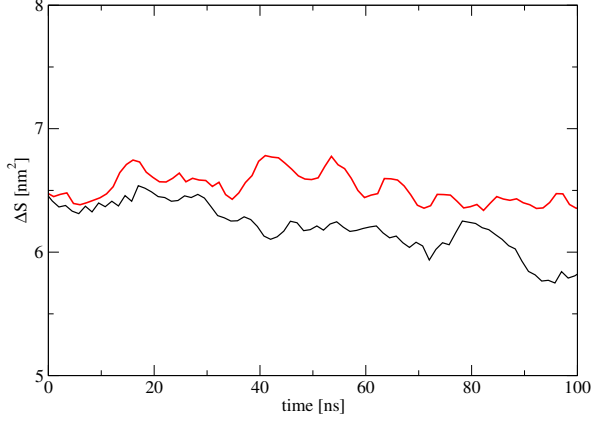


Figure 9. Time evolution of the pore area in the normal (black line) and cancer (red line) membranes under equilibrium condition at 300 K and 1 bar. The initial pores at $t = 0$ ns were performed by a shockwave impulse of 25 mPa.s and a 10 nm bubble.

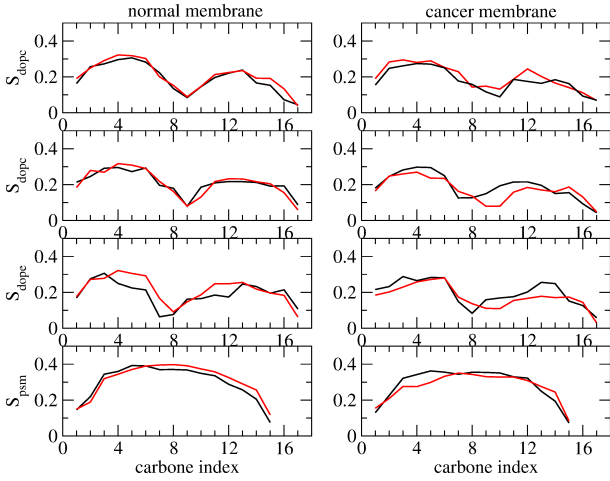


Figure 10. The order parameters averaged over the two tails sn-1 and sn-2 of four lipid types DOPC, DOPE, DOPS and PSM of the normal (left panels) and cancer (right panels) membranes. Carbon atom numbers increase in the direction of the tail termini. Shown are results before (black) and after (red) shockwave induced bubble collapse.

the pore areas are large, and the pore closure is very slow as indicated by slow relaxation of pore area to the initial equilibrium values after 50 ps.

To study the pore closure, we carry out two 100 ns MD simulations under equilibrium condition with temperature of 300 K and pressure of 1 bar for the normal and cancer membranes, starting from structures obtained at 50 ps of the shockwave simulations using shockwave impulse of 25 mPa.s and a 10 nm bubble. The initial pore areas in the normal and cancer membranes are ~ 6.5 nm [Fig.7]. As seen from Fig.9, the time evolution of

these pore areas under equilibrium condition is quite stable. The pore area in the normal membrane is decreased by $\sim 10\%$, from 6.5 to 5.8 nm, and that in the cancer membrane is decreased by only 3%, from 6.5 to 6.3 nm after 100 ns [Fig.9]. This suggests that pore closure is rather slow, and importantly, the pore in the normal membrane tends to close more rapidly than the pore in the cancer membrane. To obtain an impression on the closing speed, we simply fit the data between 20 - 100 ns shown in Fig.9 to a linear function and obtain the closing time of $\sim 1.7 \mu\text{s}$ and $5.0 \mu\text{s}$ for the normal and cancer membranes, respectively. To explain the difference in the timescale of pore closure, we recall that the equilibrium bending modulus of the cancer membrane is smaller ($K_c=8.1 \times 10^{-20}$ J) than that of the normal ($K_c=10.5 \times 10^{-20}$ J) membrane[26]. Therefore, if two membranes are stretched by the same pressure exerted by the water jet, the normal membrane will return to its original state faster than the cancer membrane, assuming that the Hooke's law is still valid. Furthermore, we calculate the order parameters, S_i , of lipids from 100 ns equilibrium trajectories after the shockwave excitation and compare results with those obtained from the equilibrium simulation without the shockwave[26]. As seen from Fig.10, the order parameter of lipids in the normal membrane before and after shockwave excitation are quite similar. In contrast, there are differences in the order parameters, especially of the DOPC and DOPE lipids in the cancer membrane before and after shockwave excitation. This confirms that the cancer membrane relaxes to equilibrium more slowly than the normal membrane.

D. Membrane response under shockwave but no bubble collapse

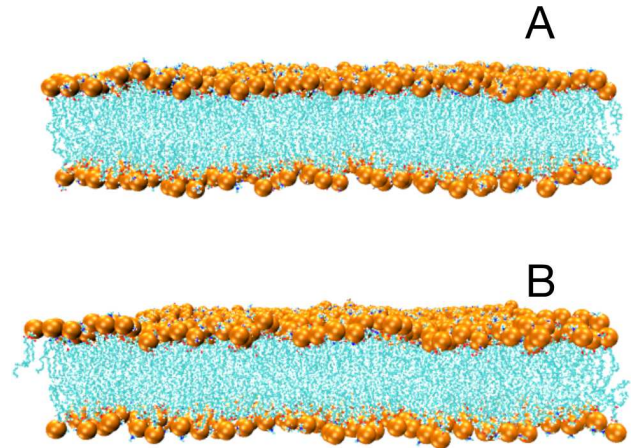


Figure 11. Snapshots taken at $t = 3$ ps from the simulation of the normal (A) and cancer (B) membranes without bubble but with a shockwave impulse of 23 mPa.s. The phosphate atoms of lipids are shown in orange and other atoms are in cyan.

Finally, to make contact to other works, we consider the impact of shockwave alone, i.e, without the bubble ($d_b = 0$ nm). To this end, we perform simulations using a relatively strong shockwave with impulse of 23 mPa.s. Figs.11(A), (B) show snapshots of the normal and cancer membranes, respectively at $t = 3$ ps when the shockwave just hits the membrane. As seen, the membranes are hardly affected, i.e, no bending or poration are observed. We increase the shockwave impulse up to 30 mPa.s but similar results are obtained. This indicates that the shockwave alone does not induce significantly structural changes in the membranes, in agreement with previous studies[12, 18, 20, 38, 39]. Furthermore, the response of the normal and cancer membranes to the shockwave is similar.

IV. DISCUSSION

We perform MD simulations of shockwave induced bubble collapse to investigate the difference in response of the normal and cancer cell membranes. These two membranes are different in the elastic moduli caused by the difference in the concentration of the phosphatidylserine lipids in the outer leaflet and the cholesterol in the bilayer[26].

We first discuss the impact of shockwave alone on two membranes. Under the shockwave excitation, a water flow is generated and uniformly directed towards the membrane, exerting an uniform pressure across all locations on the membrane, therefore the membrane is simply compressed but not perforated. Indeed, Berkowitz and colleagues performed shockwave induced bubble collapse simulations of a DPPC lipid membrane using the MARTINI coarse-grained lipid model and showed that a high intensity shockwave with an impulse of 18 mPa.s does not induce pores in the membrane[18]. Similarly, the simulation of Wei et al. for a single-component DOPC lipid membrane using the MARTINI force field showed slight compression of the membrane and no pores formation[23]. Lu et al.[20] and Wang et al.[39] studied DPPC lipid membranes using the all-atom GROMOS force field[40], and showed that the membranes are not perforated under the shockwave alone. Our simulations of multi-component lipid membranes using the all-atom CHARMM36 force field show that shockwave alone does not induce pore formation, confirming previous studies using different lipid models, compositions, and force fields[18, 20, 23, 39]. However, all these results contradict result of Espinora et al. who showed that a shockwave alone with an impulse of ~ 0.45 mPa.s could damage the membrane to an unrecoverable state[38]. This could be due to the very small size membrane studied by Espinora et al.[38].

The presence of a bubble is essential for pore formation because it focuses the uniform water flow generated by the shockwave into a water jet which hits the membrane at a focal area. The peak pressure values at this area are

very high, for example, up to 4.2 GPa in the simulation with $I = 21$ mPa.s and 10 nm bubble, which can perforate pores at the focal area. Using the piston method to generate the shockwave[41], Adhikari et al. showed that the peak pressure at the membrane is ~ 0.55 GPa in a simulation using a piston velocity of 1 km/s and a 60 nm bubble[18]. Ganzenmueller et al. performed large scale coarse-grained simulations with a piston velocity of 4.73 km/s but without a bubble and showed that the peak pressure is ~ 3 GPa[12]. In all these studies, although the peak pressure values are very high but the durations of the shockwaves are very short, therefore the values of the pressure impulses exerted on the membrane are very small [Tab.II]. We should mention that these values are much lower than an experimentally measured value impulse of 54 Ps.s which is sufficient to deliver calcein molecules into the cell but does not cause the cell death[42].

We then study the response of the membrane as a function of the shockwave impulse and bubble size in detail. Overall, our results show that the stronger the shockwave impulse or the larger the size of the bubble, the larger the pore area. This result is similar to the earlier simulations of Wei et al.[23] and Sun et al.[19] although the authors used a different, i.e, momentum mirror method to generate the shockwave, and moreover the system sizes, lipid compositions as well as the force fields are different from our simulations.

The cancer membrane studied in this work has a lower bending modulus than the normal counterpart. As a consequence, for a given shockwave impulse and bubble combination, the cancer membrane is more bent and perforated than the normal membrane. The pore area in the cancer membrane is always larger than the pore area in the normal membrane. However, we do not observe extreme cases where the cancer membrane was perforated while the normal membrane was not. This is because the bending modulus of the cancer membrane is only $\sim 22\%$ smaller than that of the normal membrane, thus the response of two membranes to the water jet is not much different. The largest differences of 20-23% in the pore areas between the normal and cancer membranes are observed for the cases with the shockwave impulses of 21-23 mPa.s and a bubble of 10 nm. We observe that increasing the shockwave impulse and/or bubble size to large values does not increase the difference in the pore area. This is because the pressure exerted by water jet on the membrane is too strong, lipids are immediately expelled from the membrane, and pores are formed without much bending of the membrane. This means that in this case the difference in the elasticity between the normal and cancer membranes does not really determine the difference in the pore areas. We show that the pore formed in the cancer membrane is closed more slowly than the pore in the normal membrane, implying that once deformed, the cancer membrane takes longer to relax to equilibrium than normal cell membrane. Again, this is because the cancer membrane has a lower bending modulus than the

normal counterpart.

As mentioned, there have been a number of simulation studies on the interaction between the shockwave and membranes[10, 11, 16–23, 39]. However, to our best knowledge there is currently only one simulation of Wei et al. who studied the response of membranes with different elasticities on the shockwave induced bubble collapse. In that work, the membrane is a single-component DOPC lipid bilayer modelled by the coarse-grained MARTINI force field. The elasticity of the DOPC membrane is varied by varying the population of the peroxidized DOPC lipids. The bending modulus of the 100% peroxide lipid membrane is $K_c = 4.3 \times 10^{-20}$ J which is about half of that of the membrane without peroxide, $K_c = 8.4 \times 10^{-20}$ J. As a consequence, the authors showed that a shockwave impulse of 127.1 mPa.s is required to perforate the 100% peroxide membrane while a stronger impulse of 161.3 mPa.s is necessary for the pore formation in the 0% peroxide membrane. This result together with our result confirm that the shockwave induced bubble collapse damage threshold for low elastic membranes is lower than that required for high elastic counterparts.

It is instructive to compare the timescale of pore formation induced by shockwave induced bubble collapse with that obtained by other excitation methods. In a previous work, we simulated the effect of stable bubble cavitation on a lipid bilayer and showed that the bubble fuses with the membrane and subsequent cavitation pulls lipid molecules out of the membrane, creating pores after ~ 30 ns[32]. In another work, we simulated the direct interaction between focused ultrasound and a lipid membrane and showed that the spatial pressure gradient between the focused and non-focused regions causes the pore formation after ~ 225 ns[43]. If the pore opening process is slow then unwanted molecules may be able to enter the cell together with drugs during the pore opening. In this context, the shockwave method is preferable because it allows rapid drug delivery into cells.

The simulation does not show large differences in the pore areas in the normal and cancer membranes because the bending moduli of two membrane models are not much different. Is this true for real biological cells? In reality, cancer cells are much softer than normal cells[24]. For example, Lekka et al. used the scanning force microscopy to exam the elasticity of normal and cancer human bladder cells, and the results show that the Young's modulus, defined as a measure of cellular deformability, of cancer cells is one order of magnitude larger as compared to healthy cells[44]. Using high-throughput optical tweezers technique, three cell lines were compared: a non-tumorigenic breast epithelial MCF10 cells, a non-motile, non-metastatic breast epithelial cancer MCF7 cells and MCF7 cells transformed with phorbol ester. The results showed a significant increase in the deformability in the transformed MCF7 cells as compared to both non-metastatic MCF10 and non-transformed MCF7 cells [45]. Further studies provide a large database of cases showing significantly larger deformability of single cancer cells

[46–48]. The very large difference in the elasticity between normal cells and cancer cells suggests that one can always be able to select a suitable range of parameters of the shockwave impulse and bubble such that cancer cells are maximally perforated while normal cells are minimally affected or even unaffected. Even if the normal cell is perforated, the pores will be closed more quickly, therefore if drugs are injected after the pores in the normal cells have closed, then drugs can only enter the cancer cells where pores are still open, i.e, the normal cells are safe.

We acknowledge that although this is a proof-of-concept work, we believe that our proposed method can be realised experimentally. Indeed, shockwave has been applied to cancer therapy. Some experimental works have shown that the shockwave can suppress tumor growth and selectively kill malignant cells[15, 49]. The technique that uses a laser-induced shockwave to drive a liquid microjet at a very speed has also been developed[50]. The gas bubbles have been widely used in ultrasound induced bubble cavitation aimed at enhancing drug delivery into cells. In this approach, ultrasound is used to induce the stable cavitation of microbubbles, generating microstreaming which exerts shear stresses on the cell membrane, resulting in pore formation or even disruption of the cell[51]. In this context, the combination of shockwave and bubble into an experimental method to rapidly and selectively perforate cancer cell membranes for drug delivery is quite doable.

V. CONCLUSION

We have performed MD simulations of shockwave induced bubble collapse on normal and cancer membrane models. We show that the combination of shockwave and bubble is essential for the pore formation in the membrane. That is, the perforation is due to the water nanojet generated by a collapse of bubble under shockwave. We show that given a combination of a shockwave and a bubble, the cancer membrane is more bent, and the pore area in the cancer membrane is larger than that in the normal membrane, because the cancer membrane is softer than the normal membrane. But the pore areas in the two membrane types become similar if the shockwave is too strong. Our simulation results could provide a proof-of-concept for the development of a new method that uses shockwave and bubble to rapidly deliver drugs into cancer cells while leaving normal cells less affected. For further development, it is important to obtain the pore area as a function of the bending modulus for various cancer cell membranes which have different elastic properties. This could provide a hint for optimising the shockwave impulse and bubble size in order to optimise drug delivery outcome. Finally, we note that the cell membranes considered in this work contain only lipid bilayers. It is necessary to include other components such as cytoskeleton which is responsible for providing struc-

tural integrity and mechanical stability. To model such complex systems, one could resort to advanced multi-scale, coarse-grained approaches[12–15]. This is our future research direction.

VI. ACKNOWLEDGMENTS

This work has been supported by the Department of Science and Technology at Ho Chi Minh City, Vietnam (grant 13/2020/HD-PQTKHCN), the European Union’s Horizon 2020 research and innovation programme under the Marie Skłodowska-Curie grant agreement No 101034407 and the CNRS. Computational support from the IDRIS, CINES, TGCC centers (project A0110712955) are acknowledged.

DATA AVAILABILITY The data that support the findings of this study are available from the corresponding author upon reasonable request.

-
- [1] S. D. Conner and S. L. Schmid, *Nature* **422**, 37 (2003).
- [2] P. Shinde, A. Kumar, Kavitha, K. Dey, L. Mohan, S. Kar, T. K. Barik, J. Sharifi-Rad, M. Nagai, and T. S. Santra, *Delivery of Drugs* **2**, 161 (2020).
- [3] P. Tyagi and Y.-C. Chuang, *Transl. Res. Biomed.* **6**, 117 (2018).
- [4] T. Kodama, A. G. Doukas, and M. R. Hamblin, *Biochim. Biophys. Acta* **1542**, 186 (2002).
- [5] L. M. Lopez-Marin, B. E. Millan-Chiu, K. Castano-Gonzalez, C. Aceves, F. Fernandez, A. Varela-Echavarría, and A. M. Loske, *J. Membr. Biol.* **250**, 41 (2017).
- [6] B. Qi, T. Yu, C. Wang, T. Wang, J. Yao, X. Zhang, P. Deng, Y. Xia, W. G. Junger, and D. Sun, *J. Exp. Clin. Cancer Res* **35**, 161 (2016).
- [7] U. Lauer, E. Burgelt, Z. Squire, K. Messmer, P. H. Hofschneider, M. Gregor, and M. Delius, *Gene Ther.* **4**, 710 (1997).
- [8] R. Murata, K. Nakagawa, and H. Moriya, *Osteoarthritis Cartilage* **15**, 1275 (2007).
- [9] G. Yao, J. Chen, Y. Duan, and X. Chen, *BioMed Research International* **2020**, 2064781 (2020).
- [10] K. Koshiyama, T. Kodama, T. Yano, and S. Fujikawa, *Biophys. J.* **91**, 2198 (2006).
- [11] A. Choubey, M. Vedadi, K. Nomura, R. K. Kalia, A. Nakano, and P. Vashishta, *Appl. Phys. Lett.* **98**, 023701 (2011).
- [12] G. C. Ganzenmueller, S. Hiermaier, and M. O. Steinhauser, *Soft Matter* **7**, 4307 (2011).
- [13] G. C. Ganzenmueller, S. Hiermaier, and M. O. Steinhauser, *PLoS One* **7**, e51989 (2012).
- [14] M. Schmidt, U. Kahlert, J. Wessolleck, D. Maciaczyk, B. Merkt, J. Maciaczyk, J. Osterholz, G. Nikkhah, and M. O. Steinhauser, *Sci. Rep.* **4**, 3849 (2014).
- [15] M. O. Steinhauser and M. Schmidt, *Soft Matter*. **10**, 4778 (2014).
- [16] K. P. Santo and M. L. Berkowitz, *J. Phys. Chem. B* **119**, 8879 (2014).
- [17] K. P. Santo and M. L. Berkowitz, *J. Chem. Phys.* **140**, 054906 (2014).
- [18] U. Adhikari, A. Goliaei, and M. L. Berkowitz, *J. Phys. Chem. B* **119**, 6225 (2015).
- [19] D. Sun, X. Lin, Z. Zhang, and N. Gu, *J. Phys. Chem. C* **120**, 18803 (2016).
- [20] X. M. Lu, B. Yuan, X. R. Zhang, K. Yang, and Y. Q. Ma, *Appl. Phys. Lett* **110**, 023701 (2017).
- [21] N. Nan, D. Si, and G. Hu, *J. Chem. Phys.* **149**, 074902 (2018).
- [22] Q. Hu, L. Zhang, and R. P. Joshi, *AIP Adv.* **9**, 045006 (2019).
- [23] T. Wei, L. Gu, M. Zhou, Y. Zhou, H. Zhang, and M. Li, *J. Phys. Chem. B* **125**, 6912 (2021).
- [24] C. Alibert, B. Goud, and J. B. Manneville, *Biol. Cell* **109**, 167 (2017).
- [25] F.-S. Quan and K. S. Kim, *Acta Biochimica et Biophysica Sinica* **48**, 865 (2016).
- [26] N. H. Linh, V. H. Man, M. S. Li, J. Wang, P. Derreumaux, and P. H. Nguyen, *Phys. Chem. Chem. Phys.* **24**, 6225 (2022).
- [27] D. Marquardt, B. Geier, and G. Pabst, *Membranes* **5**, 180 (2015).
- [28] J. Connor, C. Bucana, I. J. Fidler, and A. J. Schroit, *Proc. Natl. Acad. Sc. U.S.A* **86**, 3184 (1989).
- [29] T. Utsugi, A. J. Schroit, J. Connor, C. D. Bucana, and I. J. Fidler, *Cancer Res* **51**, 3062 (1991).
- [30] K. Simons and E. Ikonen, *Science* **290**, 1721 (2000).
- [31] H. Fu, J. Comer, W. Cai, and C. Chipot, *J. Phys. Chem. Lett.* **6**, 413 (2015).
- [32] V. H. Man, M. T. Phan, M. S. Li, P. Derreumaux, W. Junmei, N. T. Van-Oanh, P. Derreumaux, and P. H. Nguyen, *J. Phys. Chem. B* **123**, 71 (2019).
- [33] A. D. MacKerell Jr., D. Bashford, M. Bellott, R. L. Dunbrack, J. D. Evanseck, M. J. Field, S. Fischer, J. Gao, H. Guo, S. Ha, D. Joseph-McCarthy, L. Kuchnir, K. Kuczera, F. T. K. Lau, C. Mattos, S. Michnick, T. Ngo, D. T. Nguyen, B. Prodhom, W. E. R. III, B. Roux, M. Schlenkrich, J. C. Smith, R. Stote, J. Straub, M. Watanabe, J. Wiorcikiewicz-Kuczera, D. Yin, and M. Karplus, *J. Phys. Chem. B* **102**, 3586 (1998).
- [34] E. Lindahl, B. Hess, and D. van der Spoel, *J. Mol. Mod.* **7**, 306 (2001).
- [35] T. Darden, D. York, and L. Pedersen, *J. Chem. Phys.* **98**, 10089 (1993).
- [36] O. H. Ollila, H. J. Risselada, M. Louhivuori, E. Lindahl, I. Vattulainen, and S. J. Marrink, *Phys Rev Lett.* **102**, 078101 (2009).
- [37] L. S. Vermeer, B. L. de Groot, V. Reat, A. Milon, and J. Czapllicki, *Eur Biophys J* **36**, 919 (2007).

- [38] S. Espinosa, N. Asproulis, and D. Drikakis, *Microfluid Nanofluid* **16**, 613 (2013).
- [39] X. Wang, G. Tao, P. Wen, B. Ren, C. Pang, and C. Du, *J. Phys. Chem. B* **124**, 9535 (2020).
- [40] W. van Gunsteren, S. R. Billeter, A. A. Eising, P. H. Hünenberger, P. Krüger, A. E. Mark, W. Scott, and I. Tironi, *Biomolecular Simulation: The GROMOS96 Manual and User Guide*. (Vdf Hochschulverlag AG an der ETH, Zurich, 1996).
- [41] P. Wen, G. Tao, D. E. Spearot, and S. R. Phillpot, *J. Appl. Phys.* **131**, 051101 (2022).
- [42] T. Kodama, M. R. Hamblin, and A. G. Doukas, *Biophys J* **79**, 1821 (2000).
- [43] V. H. Man, M. S. Li, W. Junmei, P. Derreumaux, and P. H. Nguyen, *J. Chem. Phys.* **150**, 215101 (2019).
- [44] M. Lekka, P. Laidler, D. Gil, J. Lekki, Z. Stachura, and A. Z. Hryniewicz, *European Biophysics Journal* **28**, 312 (1999).
- [45] J. Guck, S. Schinkinger, B. Lincoln, F. Wottawah, S. Ebert, M. Romeyke, D. Lenz, H. M. Erickson, R. Ananthakrishnan, D. Mitchell, J. Kas, S. Ulvick, and C. Bilby, *Biophys. J* **88**, 3689 (2005).
- [46] E. C. Faria, N. Ma, E. Gazi, P. Gardner, M. Brown, N. W. Clarke, and R. D. Snook, *Analyst.* **133**, 1498 (2008).
- [47] W. Xu, R. Mezencev, B. Kim, L. Wang, J. McDonald, and T. Sulchek, *PLoS ONE* **7**, e46609 (2012).
- [48] M. Lekka, D. Gil, K. Pogoda, J. Dulinska-Litewka, R. Jach, J. Gostek, O. Klymenko, S. Prauzner-Bechcicki, Z. Stachura, J. Wiltowska-Zuber, K. Okon, and P. Laidler, *Arch Biochem Biophys.* **518**, 151 (2012).
- [49] F. Gamarra, F. Spelsberg, M. Dellian, and A. E. Goetz, *Int. J. Cancer.* **55**, 153 (1993).
- [50] V. Menezes, S. Kumar, and K. Takayama, *J. Appl. Phys.* **106**, 086102 (2009).
- [51] G. Peruzzi, G. Sinibaldi, G. Silvani, G. Ruocco, and C. M. Casciola, *Colloids and Surface B: Biointerfaces.* **168**, 83 (2018).